Review of Scientific Instruments

A photogrammetric method for target monitoring inside the MEG II detector

Cite as: Rev. Sci. Instrum. **92**, 043707 (2021); https://doi.org/10.1063/5.0034842
Submitted: 23 October 2020 . Accepted: 27 March 2021 . Published Online: 08 April 2021

G. Cavoto, G. Chiarello, M. Hildebrandt, A. Hofer, K. Ieki, M. Meucci, S. Milana, V. Pettinacci, F. Renga, and C. Voena

Review of Scientific Instruments ARTICLE scitation.org/journal/rsi

A photogrammetric method for target monitoring inside the MEG II detector

Cite as: Rev. Sci. Instrum. 92, 043707 (2021); doi: 10.1063/5.0034842
Submitted: 23 October 2020 • Accepted: 27 March 2021 •
Published Online: 8 April 2021

G. Cavoto,[1,a] G. Chiarello,[2] M. Hildebrandt,[3] A. Hofer,[3] K. Ieki,[4] M. Meucci,[1,a] S. Milana,[2] V. Pettinacci,[2] F. Renga,[2,b] and C. Voena[2]

AFFILIATIONS

[1] Physics Department, Sapienza Università di Roma, P.le Aldo Moro 2, 00185 Rome, Italy
[2] INFN Roma, P.le Aldo Moro 2, 00185 Rome, Italy
[3] Paul Scherrer Institut, Forschungsstrasse 111, 5232 Villigen, Switzerland
[4] ICEPP, The University of Tokyo, 7-3-1 Hongo, Bunkyo-ku, Tokyo 113-0033, Japan

[a] **Also at:** INFN Roma, P.le Aldo Moro 2, 00185 Rome, Italy.
[b] **Author to whom correspondence should be addressed:** francesco.renga@roma1.infn.it

ABSTRACT

An automatic target monitoring method based on photographs taken by a CMOS photo-camera has been developed for the MEG II detector. The technique could be adapted for other fixed-target experiments requiring good knowledge of their target position to avoid biases and systematic errors in measuring the trajectories of the outcoming particles. A CMOS-based, high resolution, high radiation tolerant, and high magnetic field resistant photo-camera was mounted inside the MEG II detector at the Paul Scherrer Institute (Switzerland). MEG II is used to search for lepton flavor violation in muon decays. The photogrammetric method's challenges, affecting measurements of low momentum particles' tracks, are the high magnetic field of the spectrometer, high radiation levels, tight space constraints, and the need to limit the material budget in the tracking volume. The camera is focused on the dot pattern drawn on the thin MEG II target, about 1 m away from the detector endcaps where the photo-camera is placed. Target movements and deformations are monitored by comparing images of the dots taken at various times during the measurement. The images are acquired with a Raspberry board and analyzed using custom software. Global alignment to the spectrometer is guaranteed by corner cubes placed on the target support. As a result, the target monitoring fulfills the needs of the experiment.

I. INTRODUCTION

Magnetic spectrometers used to determine the momentum of charged particles in high-energy physics experiments (HEPs) require an accurate reconstruction of the trajectory of the particle over a relatively large volume. This is usually achieved by measuring with high precision various positions in space and then connecting them to obtain the best evaluation of the trajectory. The relative uncertainty in the momentum of a charged particle is equal to the relative uncertainty in the curvature of the trajectory. Typical particle detectors used in HEP spectrometers are gaseous drift chambers, time-projection chambers, etc., which can be made of sub-elements that require an accurate relative alignment. Moreover, it is important to measure their relative position with respect to other elements, including a production target where the charged particles under study are emerging from. Generally, to reach the desired performances, high accuracy of the mechanical assembly is required. However, due to the apparatuses' complexity, these measurements are often difficult and *ad hoc* solutions need to be developed to reach sub-millimeter alignment of the critical elements. Space constraints, strong magnetic fields, and high radiation levels add to the list of challenges. Different solutions were adopted in HEP experiments, some of them exploiting optical detection of patterns printed on the detectors themselves.[1] Similar challenges arise in high-power laser experiments, where targets have to be replaced in a fast turnaround time.[2]

In this paper, we describe a method that has been developed to monitor the position of the muon stopping target in the MEG II experiment at the Paul Scherrer Institute (PSI, Villigen, Switzerland). The method is based on a photogrammetric survey of a dot

pattern printed on the target itself. The main challenges of this approach are connected to the use of photo-cameras in an environment with a high magnetic field and high radiation. Since these conditions are common in HEP experiments, the approach may be of interest to other experiments.

The MEG II experiment[3] is an upgrade of the MEG experiment, which sets the best world limit[4] on the decay of a muon into a positron and a photon, $\mu^+ \to e^+\gamma$. This decay is being searched for since the discovery of the muon and was never observed. Indeed, it is practically forbidden in the Standard Model of particle physics, and its discovery would be the demonstration of new physics effects. If the decay is not observed, MEG II is expected to set an upper limit of 6×10^{-14} on its branching ratio, further constraining theoretical models for physics beyond the Standard Model. The future availability of higher intensity muon beams could further improve the experimental sensitivity to this decay.[5]

The search for $\mu^+ \to e^+\gamma$ requires stopping a large amount of muons, detecting a positron and a photon emerging in coincidence from the stopping target, and reconstructing their kinematics. In the MEG II experiment, the PSI beam of positive muons (7×10^7 muons/s) is stopped in a thin plastic target at the center of the MEG II detector. It includes a spectrometer to measure the trajectory of the 52.8 MeV positrons possibly produced in the $\mu^+ \to e^+\gamma$ decay and a Liquid Xenon (LXe) calorimeter to detect the photon (plus some auxiliary detectors). The MEG II magnetic spectrometer is composed of a single volume multi-wire drift chamber[6,7] in a solenoidal gradient magnetic field. One of the dominant systematic errors in the evaluation of the yield of $\mu^+ \to e^+\gamma$ events in the previous MEG experiment was due to the uncertainty in the target position with respect to the spectrometer and its internal deformation, which could not be measured directly. In order to identify a $\mu^+ \to e^+\gamma$ event, it is necessary to measure the angles of the e^+ trajectory at the point where the muon has decayed (muon decay point). This is done by back-propagating the trajectory measured by the spectrometer up to the target region, which is assumed to be a planar surface. The MEG II spectrometer is expected to provide a precision of about 5 mrad on the θ (polar) and ϕ (azimuthal) angles of the positron trajectory at the target. In the MEG II reference system, z is the axis along the beam direction. A precise knowledge of the target position is then required: given a radius of curvature of about 13 cm for the e^+ trajectory in $\mu^+ \to e^+\gamma$ events, a displacement of the target by 500 μm along the direction normal to it implies a systematic deviation of about 4 mrad in the measured positron ϕ angle for $\phi = 0$. An even larger effect is expected for non-zero values of ϕ. Figure 1 shows the effect of a displacement of the target in the direction orthogonal to its plane on the reconstructed track angles. It can be seen that the impact on the azimuthal angle can be sizable, while the effect on the polar angle is negligible. Moreover, deformations of the target planarity, which produce a similar effect, were observed through the MEG data-taking. The uncertainty in the target position and deformation was in fact the dominant systematic error in the MEG result. It caused a 5% variation of the upper limit on the branching fraction, while other contributions were below 1%.

During the MEG data-taking, the position of the target plane was measured every run period (i.e., every year) with an optical survey of crosses depicted on the target plane. Unfortunately, the small field of view available for triangulation, combined with the distance of the target from the closest accessible point of view (about 1 m), prevented from achieving an accuracy better than 1 mm. Target position monitoring over long data-taking periods was also possible by reconstructing the position of a few holes bored on the target itself. A map of the reconstructed muon decay points on the target clearly showed the position of such holes. If the target position assumed in the trajectory reconstruction procedure is not exact, holes will artificially appear at different positions for different e^+ angles. This allowed us to reconstruct deviations of the target position from the nominal one. This method was also effective to catch and correct the deformation of the target planarity. On the other hand, it required a large amount of data so that it could only be used to monitor the average target position over a few months of data-taking. However, the target was removed far from its working position at least every week to perform the calibration of the LXe detector. A pneumatic system was used for this, but it did not ensure a micrometric repeatability of the target positioning. While the target hole technique was precise enough for the MEG experiment, the improved resolutions of the MEG II positron spectrometer imposed the development of an alternative method. It must ensure a more frequent monitoring of the target position over the data-taking period and has to be able to resolve displacements equivalent to about 100 μm along the direction normal to the target plane.

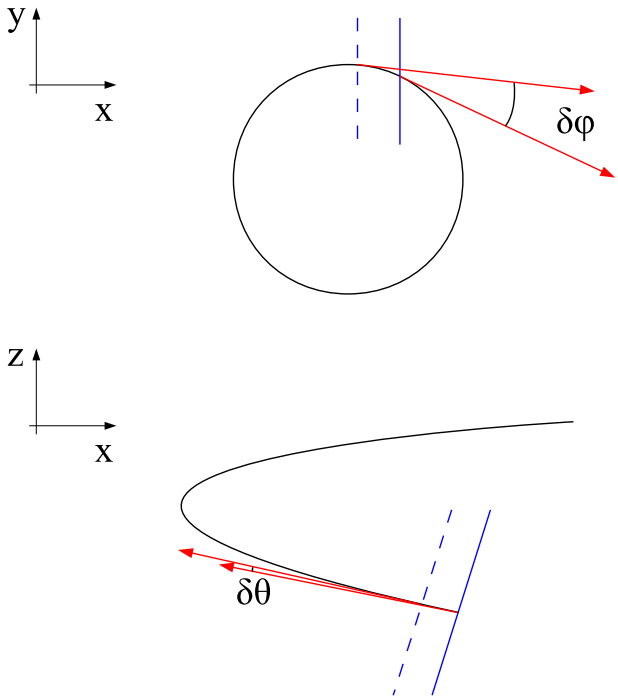

FIG. 1. Sketch (not in scale) of the impact of a target displacement on the reconstructed track angles. The dashed (full) segment represents the assumed (true) target projection in the corresponding plane. Top: projection on the x–y plane, where the positron trajectory projection is a circle. $\delta\phi$ is the difference between the true and the reconstructed azimuthal angle of the track. Bottom: projection on the x–z plane, where the curve represents the positron trajectory projection in this plane. $\delta\theta$ is the difference between the true and the reconstructed polar angle of the track.

We here present a photogrammetric approach that will employ a digital CMOS photo-camera to take pictures of a pattern drawn on the target itself. The photo-camera will be placed in the inner cavity of the MEG II cylindrical drift chamber where muons travel along to reach the target. The engineering of the photo-camera mounting will play a key role: it must ensure dimensional mechanical stability over time in a high radiation environment and sufficient rigidity to adequately support the instrumentation. The support—although necessarily compact in size—should avoid deformation and should not be affected by the high active magnetic field. All this requires a study of non-magnetic materials to be used. Moreover, the total amount of material should be kept as small as possible because positrons hitting the system can produce photon background in the calorimeter. We will show that the photo-camera can be installed without affecting the muon propagation and the magnetic field. Together with the photo-camera described in this paper, a different photo-camera was installed and tested inside the MEG II detector.[8] Here, we propose different optical configurations and algorithms. Moreover, a systematic analysis of the achievable resolution, obtained in a controlled bench-top setup, will be presented.

II. THE PHOTOGRAMMETRIC APPROACH

A. The experimental setup

The MEG II target is an elliptical foil (length of 270 mm and height of 66 mm) with 174 μm average thickness, made of scintillating material. Its normal direction lies on the horizontal plane and forms an angle of 75° with respect to the z axis. The target foil is supported by two hollow carbon fiber (CF) frames. A pattern of white dots, superimposed on a black background, is printed on both the frame and the foil. The dots are elliptical with a height and a width of 0.51 and 1.52 mm on the target and 0.42 and 1.27 mm on the frame. The ratio of the two axes is chosen in such a way that, considering the target orientation and the photo-camera position, the dots look circular in the picture. This dot pattern has been found superior to others including white lines with black contours. Figure 2 shows a picture of the MEG II target. The dots are imaged with a digital CMOS photo-camera (IDS, model UI-3282SE), with a Sony IMX264 sensor having 2456×2054 pixel^2 of 3.5 μm size, for a total sensor size of 8.473×7.086 mm^2. A TUSS optical system, model LVK7518, with a focal length of 75 mm and a maximum aperture of $f/1.8$ is used. The read-out of the photo-camera uses a Raspberry board, hosted in a crate close to the apparatus, which uses the USB3 protocol for communication. Previous tests found that the Ethernet communication is not compatible with the MEG II high magnetic field. The USB cable from the photo-camera, which also provides power, exits the internal volume via a feedthrough present on a connection flange, sealed with glue. A LED system supported independently illuminates the target during the data-taking period.

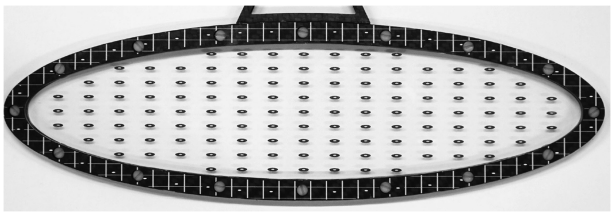

FIG. 2. The MEG II target with the dot pattern on the foil and the frame.

The value of the magnetic field at the position where the photo-camera is installed along the z axis is about 0.8 T. The magnetic force applied on the photo-camera assembly has been evaluated, and the support design has been optimized through a dedicated topological analysis in terms of material and geometry. This ensures a proper rigidity during the measurement stage. The possible interference induced by the photo-camera to the magnetic field was measured with Hall probes and found to be negligible. The photo-camera was placed on an *ad hoc* support, approximately in the nominal position, which hosted a Hall cube with six sensors (two for each direction). The observed deviations from the total field in the presence of the photo-camera were found to be less than 0.6%, 0.2%, and 0.2% in the x, y, and z directions, respectively.

To evaluate the effect of radiation damage, a photo-camera with the same sensor was left installed for more than one month during the 2017 MEG II engineering run. Although an increase in the number of hot pixels was observed, the effect is far too low to affect significantly the performances of the measurement system.

In conclusion, we are confident that the final photo-camera will work inside the COBRA magnetic field, will not affect the field itself, and will remain operative for the expected time of MEG II data-taking (three years).

The photogrammetric approach is based on the repetition of several measurements of the same points at different times. Therefore, the stability of the photo-camera mounting is crucial. Furthermore, the correct positioning is fundamental even to avoid any interference with the muon beam entering the multi-wire chamber and other equipment installed in that area. The space allocated for the instrumentation is outside the tracking volume, in order to not interfere with the positron detection. A clearance of 80 mm around the beam axis was left in order to not intersect the beam halo. Within the allowed space, it was necessary to define a system capable of aiming with extreme precision at the center of the target. Given the small space available, it was not possible to insert pointing adjustment elements, and a solution with a fixed setup was chosen. Considering also the need for inserting as little material as possible and the complexity of the shape, it was chosen to realize it through an additive manufacturing technology. Therefore, after testing a 3D printed polycarbonate prototype, the photo-camera support has been realized in Carbon Fiber (CF) Reinforced Composite material, exploiting one of the most innovative techniques emerging from the additive manufacturing global market. The CF structure was chosen in order to physically couple only materials with similar thermal and mechanical properties (the support plate of the chamber was made of CF as well). Moreover, it is sufficiently rigid to support the weight of the equipment (about 1 kg overall) without introducing deformations that may influence the pointing on the target. An additional arm was added to it for a correct routing of the power and reading cables toward the bottom of the chamber to avoid interference with the beam. This support has been used for the 2019 MEG II engineering run.

In order to improve the stiffness of the support, a new support has been realized in aluminum alloy 6060, always via additive manufacturing (direct metal laser melting process on a powder bed). This enhances also the related mounting screw pattern and reduces

the effect of instantaneous deformation when the magnetic field is switched on. The shape of the new aluminum support is the result of a topological optimization aimed at exploiting the larger rigidity of aluminum and only introducing the strictly necessary material. This innovative interface has been mounted on the real setup in preparation for the 2020 engineering run.

The support is fixed to the system for the target motion at a distance of about 1100 mm from the origin of the z axis, in correspondence with the multi-wire chamber end-plate. The transverse distance from the z axis is about 120 mm, with an angle of 6.3° with respect to the z axis. As a result, the photo-camera frames an area of about $110 \times 92\ \text{mm}^2$ around the target center, which is enough to image the entire target and its support frame. A picture of the photo-camera on the final Al support, installed in the MEG II detector, and a CAD detail are shown in Fig. 3.

To have the largest possible portion of the target reasonably in focus, an aperture of f/16 was used, providing a large enough depth of field. Given these conditions, an exposure of 750 ms was chosen in order to optimize the use of the sensor's dynamic range for the best contrast.

B. The method

The pattern of dots can be reproduced by the photo-camera, and the position of dots on the picture can be determined with standard image processing algorithms. If the target moves between two successive photo-camera shoots, the position of these patterns in the picture will change. A measurement of this displacement would allow us to measure the corresponding displacement of the target with respect to its original position. Given the size of the target to be imaged and the resolution of our photo-camera, 1 pixel in the image corresponds to a distance of a few tens of μm on the target. Moreover, since imaging algorithms allow us to reach a sub-pixel precision on the position of dot patterns, the goal of determining displacements below 100 μm in the transverse coordinates with respect to the optical axis is within reach. Displacements along the optical axis can be detected considering that the distance d between two points on the target translates into a distance d_I between two points on the image plane according to the magnification (M) formula

$$\frac{d_I}{d} = M = \frac{f}{f - L}, \tag{1}$$

where f is the focal length and L is the distance of the target from the center of the photo-camera's optical system. Hence, a movement along the optical axis (i.e., a change in L) can be detected as a change in d_I. As we will show later, this approach can obtain the required resolution also for the coordinate transverse to the optical axis.

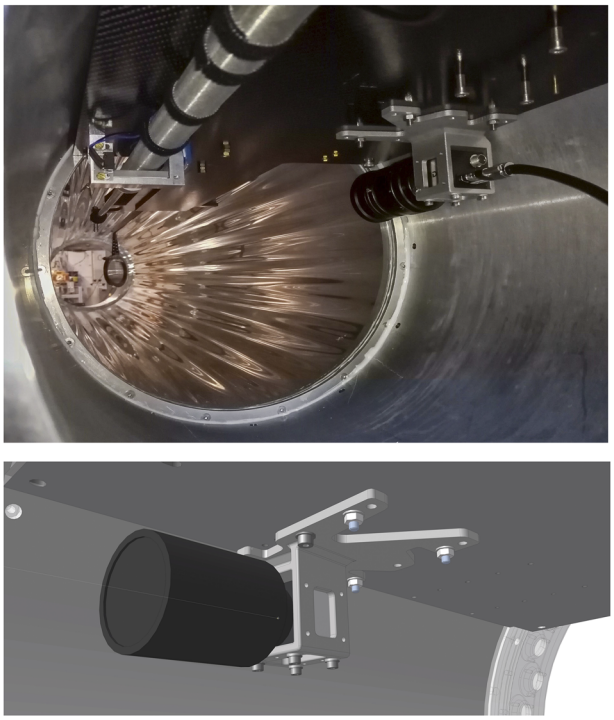

FIG. 3. Picture (upper plot) and CAD detail (lower plot) of the installation of the photo-camera with the final Al support in the inner cavity of the cylindrical drift chamber.

III. THE TARGET POSITION MEASUREMENT ALGORITHM

In this section, we describe in detail the algorithms used to determine the dot positions within the photo-camera image and to use the measured positions to extract the target position by means of a χ^2 fit.

A. Dot position measurements

The dot positions are determined in a three-step procedure using standard image processing algorithms, as shown in Fig. 4. At first, a region of interest is automatically defined around each dot based on its expected position. A Canny edge detection algorithm[9] is applied to build an image of the dot edges. Second, a circular Hough transform[10] is applied to find which pixels belong to the edge between the black contour and the white dot. Finally, a circumference is used to interpolate the positions of these pixels with a χ^2 minimization assuming 1 pixel uncertainty. The result of this fit procedure provides a measurement of the center of the white dot in the image. As an alternative approach, we evaluate the center of gravity of the picture light intensity to determine the center of the white dot, obtaining consistent results.

B. Target position and orientation measurement

If the target and photo-camera positions are known, the positions of the dots on the photo-camera image can be inferred with simple arguments of geometrical optics. In particular, given the center of the optical system, rays can be traced from a dot position on the target, through the optical center, to the sensor plane, giving the dot position in the image. With respect to the use of first-order optical relationships, this approach minimizes the systematic uncertainties. They might be introduced by the target inclination, causing the dots far from the center of the target to be slightly out of focus.

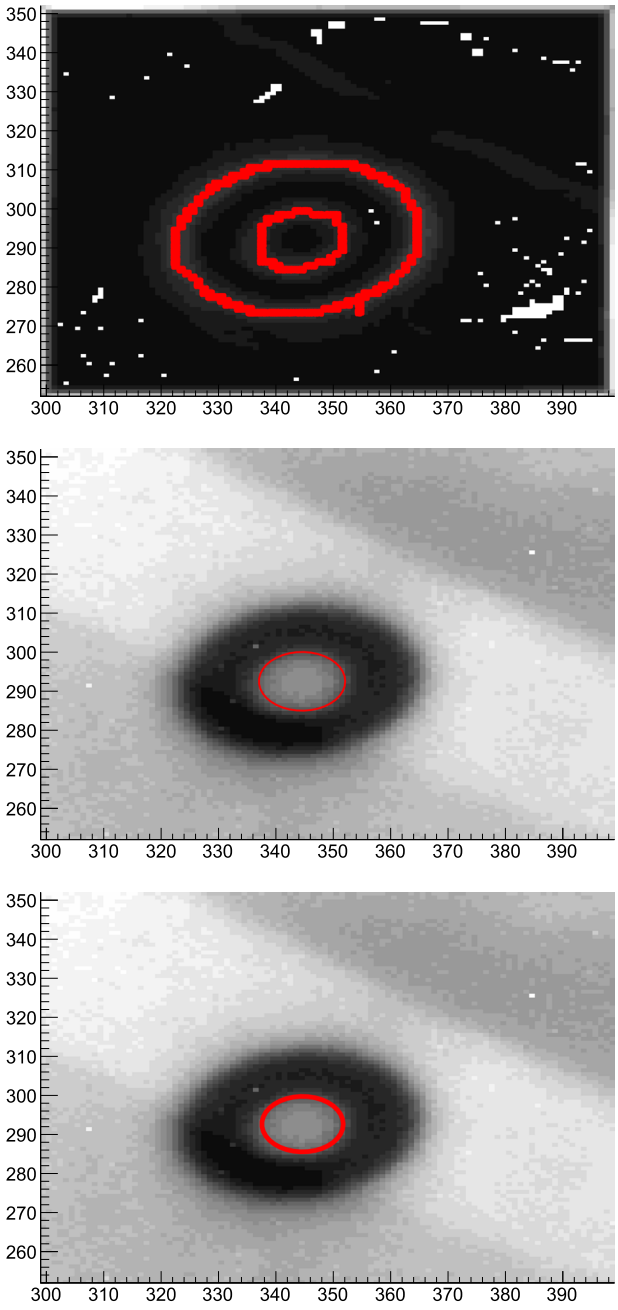

FIG. 4. Three-step procedure for determination of the dot position: edge detection with the Canny algorithm (top). Identification of the white dot contour with a Hough transform (middle). χ^2 fit for a precise determination of the dot center (bottom).

The procedure can by formally described as an operator $\mathcal{T}$ acting on the three-dimensional position $\mathbf{r}_i = (x_i, y_i, z_i)$ of the real ith dot in the MEG II reference frame and producing a two-dimensional position $\mathbf{s}_i = (p_i^x, p_i^y)$ on the sensor,

$$\mathbf{s}_i = \mathcal{T}(\mathbf{r}_i). \tag{2}$$

The operator $\mathcal{T}$ has seven parameters: the position of the optical center (three parameters), the independent components of the unit vector of the optical axis (two parameters), the orientation of the sensor around the optical axis (one parameter), and the distance of the sensor from the center of the optical system (one parameter). The positions (p_i^x, p_i^y) are measured in units of number of pixels. The dot position in the MEG II reference frame, $\mathbf{r}_i$, can be derived from the dot positions in an arbitrarily defined target reference frame, $\mathbf{t}_i = (u_i, v_i, w_i)$,

$$\mathbf{r}_i = R \cdot \mathbf{t}_i + \mathbf{T}, \tag{3}$$

where R is a rotation matrix and $\mathbf{T}$ is a translation vector. If we place the center of the target reference frame at the center of the target and we orient the first and second components of $\mathbf{t}_i$ along the major and minor axes, respectively, the vector $\mathbf{T}$ gives the center of the target in the MEG II reference frame, while the matrix R gives the target orientation. Hence, the knowledge of the corresponding six parameters (the three components of the translation vector and the three Euler angles of the rotation matrix) is sufficient to measure the target position in the MEG II reference frame.

A χ^2 function of the measured dot positions in the image with respect to the expected positions from the target orientation and the geometrical optics can be defined as

$$\chi^2 = \sum_i [\mathbf{s}_i - \mathcal{T}(R \cdot \mathbf{t}_i + \mathbf{T})]^2. \tag{4}$$

The parameters of $\mathcal{T}$ and the dot position in the target reference frame can be inferred from surveys performed at the beginning of the data-taking period, as we will explain below, so that the parameters of R and $\mathbf{T}$ (and hence the target position) can be determined by minimizing this χ^2.

The target is assumed to be perfectly planar when installed ($w_i = 0$ for any i). If a deformation occurs during the MEG II data-taking run, it can be parameterized by an additional operator $\mathcal{Z}$ acting on the original positions $\mathbf{t}_i$. The χ^2 becomes

$$\chi^2 = \sum_i [\mathbf{s}_i - \mathcal{T}(R \cdot \mathcal{Z}(\mathbf{t}_i) + \mathbf{T})]^2, \tag{5}$$

and it will be minimized as a function of the parameters of R, $\mathbf{T}$, and $\mathcal{Z}$ in order to determine the target position, its orientation, and its deformation.

The operator $\mathcal{Z}$ is parameterized by means of the Zernike polynomials,[11] which are defined in a 2D system of polar coordinates with $\rho \leq 1$ as

$$Z_n^m(\rho, \phi) = R_n^m(\rho) \cos(m\phi), \tag{6}$$

$$Z_n^{-m}(\rho, \phi) = R_n^m(\rho) \sin(m\phi), \tag{7}$$

where m and n are non-negative integers with $n \geq m$ and

$$R_n^m(\rho) = \sum_{k=0}^{\frac{n-m}{2}} \frac{(-1)^k (n-k)!}{k!\left(\frac{n+m}{2}-k\right)!\left(\frac{n-m}{2}-k\right)!} \rho^{n-2k}. \tag{8}$$

The first non-null radial polynomials are

$$R_0^0(\rho) = 1, \tag{9}$$

$$R_1^1(\rho) = \rho, \tag{10}$$

$$R_2^0(\rho) = 2\rho^2 - 1, \tag{11}$$

$$R_2^2(\rho) = \rho^2, \tag{12}$$

$$R_3^1(\rho) = 3\rho^3 - 2\rho, \tag{13}$$

$$R_3^3(\rho) = \rho^3. \tag{14}$$

In the local (u, v, w) reference frame, in order to describe a deformation of the target that is constrained to be null at the border, thanks to the stiffness of the target frame, we define

$$\rho = \sqrt{(u/a)^2 + (v/b)^2}, \tag{15}$$

where a and b are the major and minor semi-axes of the target ellipse, and we use the following parameterization:

$$\mathscr{Z}(u, v, w) = (u, v, w(u, v)), \tag{16}$$

with

$$w(u, v) = \sum_{n,m} \left[A_n^m \zeta_n^m(u, v) + A_n^{-m} \zeta_n^{-m}(u, v) \right], \tag{17}$$

$$\zeta_n^{\pm m}(u, v) = \frac{1}{2} \left[Z_n^{\pm m}(\rho, \phi) - Z_{n+2}^{\pm m}(\rho, \phi) \right]. \tag{18}$$

The first term of the series is

$$w(u, v) = A_0^0 \cdot \frac{1}{2} \left[Z_0^0(\rho, \phi) - Z_2^0(\rho, \phi) \right] = A_0^0 \cdot (1 - \rho^2), \tag{19}$$

which describes a paraboloidal deformation.

C. Operational procedure

The positions of the dots in the target reference frame can be determined by a bench-top survey of the target foil, with an accuracy much better than 100 μm. Conversely, the position and orientation of the photo-camera (and hence the parameters of the operator $\mathscr{T}$) are not known with enough precision. To overcome this difficulty, we proceed as follows. The target position at the beginning of a MEG II data-taking run will be precisely determined, with improved accuracy with respect to MEG, thanks to reflectors that are installed on the target frame for a laser survey. Immediately after, a set of pictures is taken (*reference pictures*). We can assume that the position, orientation, and shape of the target (and hence the parameters of R, $\mathbf{T}$, and $\mathscr{Z}$) are known for these pictures, thanks to the recent surveys. Hence, they can be fixed and the χ^2 can be minimized with respect to the seven parameters of $\mathscr{T}$. It provides a precise determination of these parameters. When a new measurement of the target position is needed using the photogrammetric method, a new picture is taken, and in this case, the parameters of $\mathscr{T}$ are fixed from the reference fit, while the parameters of R, $\mathbf{T}$, and $\mathscr{Z}$ are fitted.

In order to make the procedure more robust against systematic effects associated with the inaccuracy of the optical model and the initial conditions of the target, when fitting the new pictures, Eq. (5) is in fact replaced by

$$\chi^2 = \sum_i \left\{ (\mathbf{s}_i - \mathbf{s}_i^0) - \left[\mathscr{T}(R \cdot \mathscr{Z}(\mathbf{t}_i) + \mathbf{T}) - (\mathscr{T}(R^0 \cdot \mathscr{Z}^0(\mathbf{t}_i) + \mathbf{T}^0) \right] \right\}^2, \tag{20}$$

where $\mathbf{s}_i^0$ are measured and R^0, $\mathbf{T}^0$, and $\mathscr{Z}^0$ are fitted from the reference picture. In practice, the fit to the target position is replaced by a fit to the target displacement. Anyway, the fitted parameters of R, $\mathbf{T}$, and $\mathscr{Z}$ are still referred to the global MEG II reference frame for an easy interface to the MEG II reconstruction software.

An estimate of the uncertainty in the measured position of the dots is given by the minimum χ^2 divided by the number of degrees of freedom in the fit. It gives typically an error slightly below 1 pixel when the definition of Eq. (5) is used. It includes any possible inaccuracy in the optical model and aplanarity of the target. The error goes down to $\frac{1}{3}$ of a pixel when Eq. (20) is used, demonstrating the superior robustness of this approach against these inaccuracies.

Typically, a few dots per picture cannot be measured properly by the automatic procedure. They could be mostly recovered with a manual procedure by refining the regions of interest used to find and fit the dots. However, their impact is so small that we decided to simply remove a dot from the fit when its contribution to the χ^2 is larger than $25\sigma^2$, according to the estimate of the uncertainty described above.

It should also be stressed that several reference pictures need to be taken at the beginning of the data-taking period in order to reduce the statistical uncertainty in the estimate of the parameters of $\mathscr{T}$ to a negligible level. On the other hand, the χ^2 defined in Eq. (20) requires a single reference picture. For this reason, we adopted the following procedure. One of the reference pictures is taken and used to get a preliminary estimate of the parameters of $\mathscr{T}$. This is used to fit for R, $\mathbf{T}$, and $\mathscr{Z}$ in the other reference pictures. Since the target did not move in between, one would expect to get zero displacements on average. Instead, statistical fluctuations in the first picture can be observed as an average fake displacement in the other pictures. The picture producing the minimum average displacements when used as the reference is taken as the single reference picture for the whole data-taking period.

IV. BENCH-TOP TESTS

A test of the full procedure was performed by installing the photo-camera, a LED, and a target mock-up on an optical table, with the target mounted on a 2.5 μm position accuracy linear stage.

The assembly has been arranged in order to reproduce accurately the real setup installed inside the experiment. Exploiting 3D printing technologies available at INFN Roma Mechanical Workshop, precise polycarbonate mechanical supports have been designed and produced. They are able to hold all components in the correct relative positions between themselves and to interface properly the optical table and the installed linear stage. The photo-camera, instead, is fixed to the optical table using Al supports in order to reduce thermal deformations. A temperature sensor has been installed nearby the target for temperature monitoring

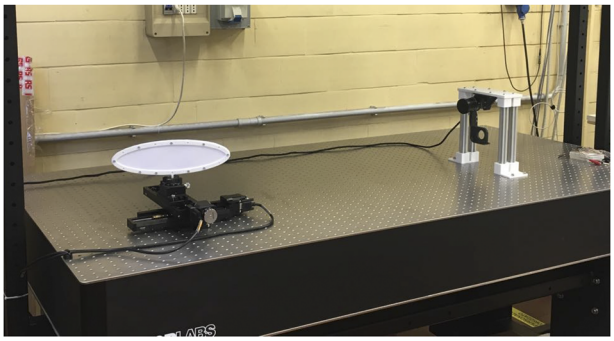

FIG. 5. Picture of the experimental setup for the bench-top test of the photogrammetric system.

while the environmental temperature is kept almost constant by air conditioning. Figure 5 shows the installed setup.

A position scan was performed independently along the x and z axes using the linear stages. This was used to evaluate the precision to which shifts in the target position can be determined.

In this test setup, we could not vary the target along the y direction, but it should be noted that such movements have no impact on the track angle measurements in the MEG II experiment.

Before each scan, ten pictures without moving the stages were taken, and one of them was chosen to serve as the reference picture, as described in Sec. III C. In this setup, the initial coordinates of the target center are assumed to be (0, 0, 0); thus, the fit returns the coordinates T_x, T_y, and T_z after the target movements.

Figures 6–8 show the fitted T_x, T_y, and T_z as a function of the true T_x in the X scan. The pictures have been taken over ~ 6 h in a random order with respect to the true shifts so that time-dependent and shift-dependent biases mix incoherently and can thus be checked independently. Linear fits have been performed to the distributions, and the errors in the fitted shifts have been estimated by means of linear regression in the case of the fitted T_x. The

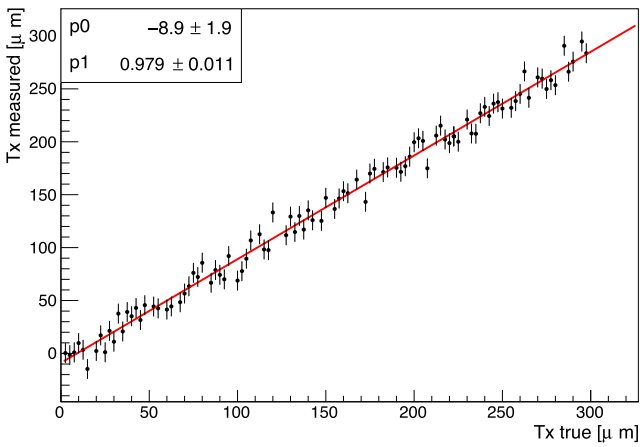

FIG. 6. T_x fitted vs true T_x in the X scan described in the text. A linear fit is superimposed.

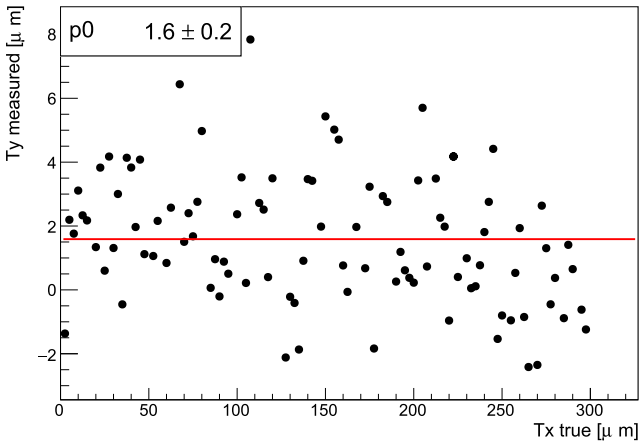

FIG. 7. T_y fitted vs true T_x in the X scan described in the text. A constant fit is superimposed.

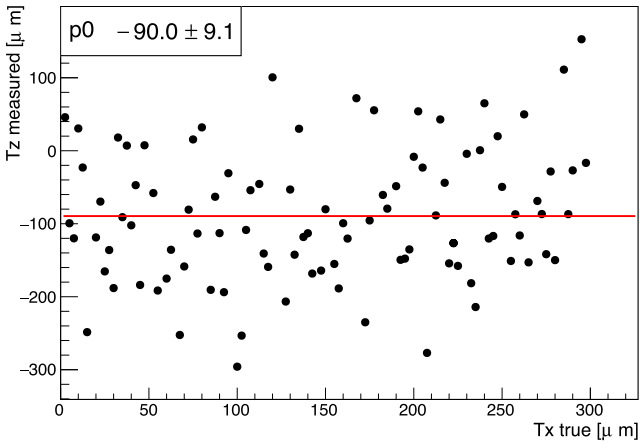

FIG. 8. T_z fitted vs true T_x in the X scan described in the text. A constant fit is superimposed.

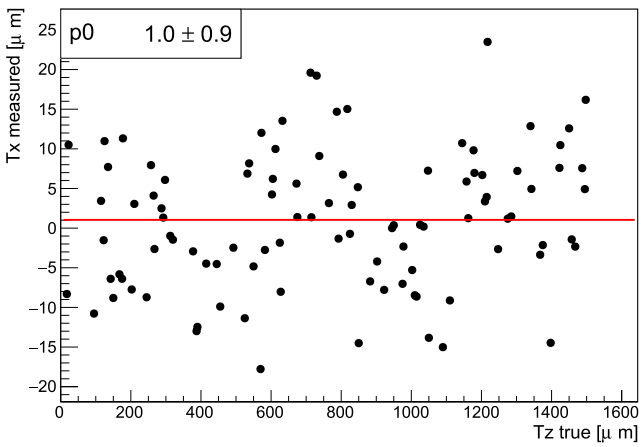

FIG. 9. T_x fitted vs true T_z in the Z scan described in the text. A constant fit is superimposed.

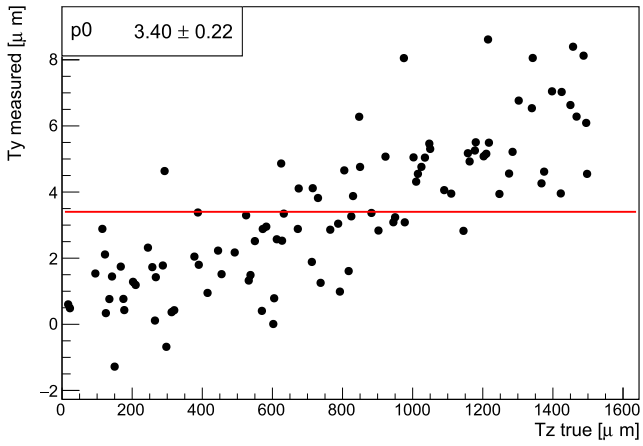

FIG. 10. T_y fitted vs true T_z in the Z scan described in the text. A constant fit is superimposed.

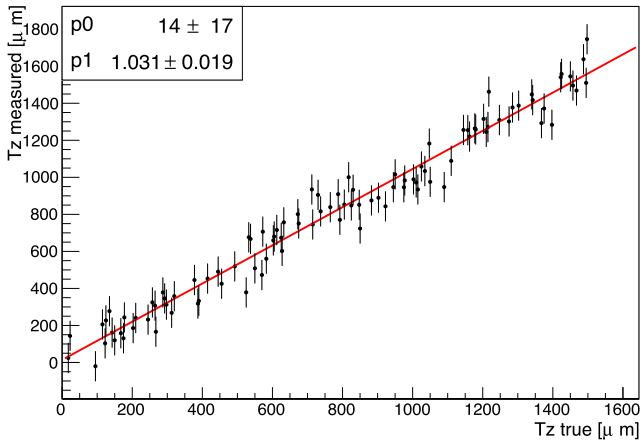

FIG. 11. T_z fitted vs true T_z in the Z scan described in the text. A linear fit is superimposed.

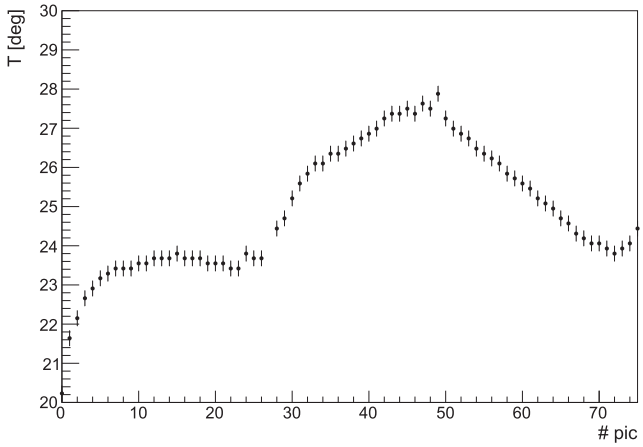

FIG. 12. Temperature vs time during the data-taking period without moving the stages.

resulting uncertainty in T_x is $\sigma(T_x) = 12\,\mu$m. Given that the direction transverse to the target plane is almost coincident with the X axis, we can conclude that we fully satisfy our precision requirements. The angular coefficients and the intercept are consistent with 1 and 0, as expected. A bias in T_z is observed, which is significantly

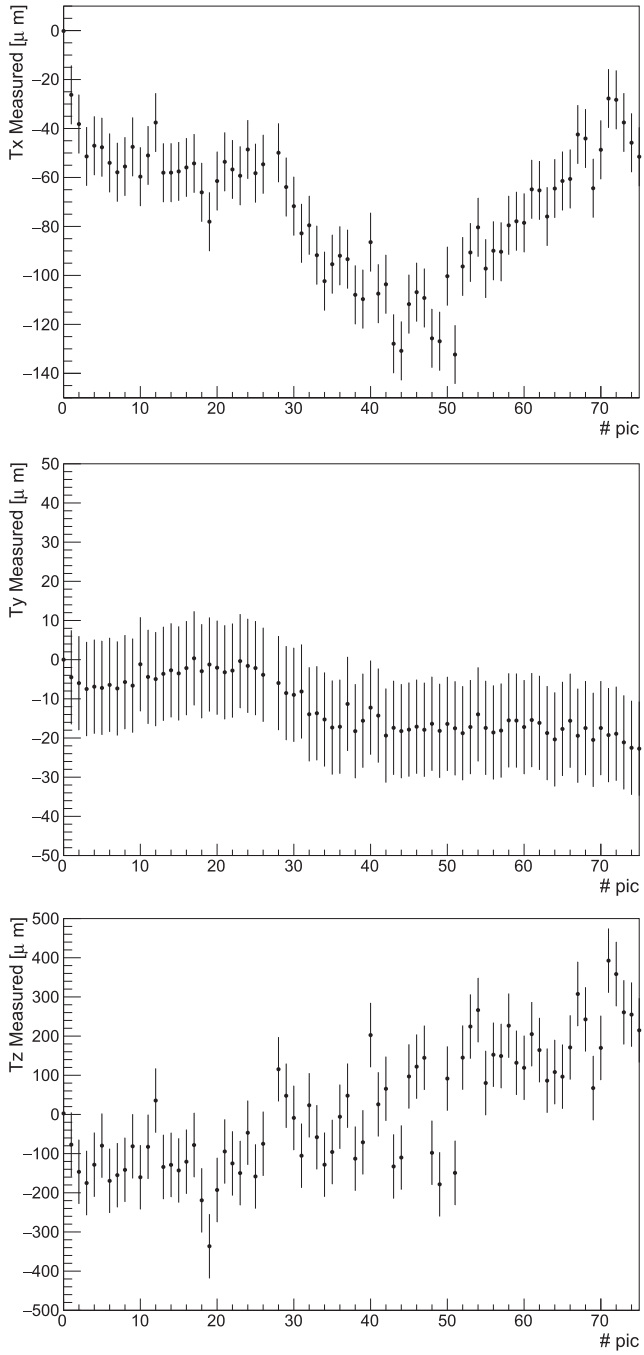

FIG. 13. Fitted T_x (upper plot), T_y (middle plot), T_z (lower plot) for the pictures taken without moving the stages.

different from 0 but still within the requirements. It is probably due to the residual uncertainty of the reference picture.

Figures 9–11 show the fitted T_x, T_y, T_z as a function of the true T_z in the Z scan. The pictures have been taken over ~ 6 h, again in a random order with respect to the true shifts. Linear fits have been performed to the distributions, and the error in the fitted T_z has been estimated by means of linear regression. The resulting uncertainty in T_z is $\sigma(T_z) = 82\,\mu$m. The angular coefficients and the intercept are consistent with 1 and 0, as expected, also in this case.

The dependency of the fitted position of the target as a function of the environmental temperature changes has been observed by taking 75 pictures in 30 min without moving the stages. Figure 12 shows the variation of the temperature vs time during the data-taking period, while Fig. 13 shows the fitted T_x, T_y, T_z from the reference picture. In these figures, the errors estimated from the X and Z scans described previously have been assumed in T_x and T_z, while the error in T_y has been assumed equal to the error in T_x although this is probably an overestimation, as was computed in a configuration where the stage was moved.

We observed a correlation of the shifts to the temperature, which is clear in T_x but can also be perceived in T_y and T_z. Looking at fixed reference points in the background of the pictures, we concluded that this dependence is due to real deformations of the target, not a change in the photo-camera position or response. Unfortunately, the poor stiffness of the target frame used in this test prevents from fitting the deformations with the Zernike polynomial approach described above. Moreover, we cannot know *a priori* the amount of deformation induced by the temperature changes. It makes not possible to give a robust estimate of the sensitivity to these deformations. Nonetheless, this result clearly demonstrates the possibility of monitoring these kinds of effects with a precision below 100 μm in all coordinates.

A study of the correlations among the fitted parameters was also performed. An example of the correlation matrix extracted from one of the fits is shown in Table I. Very large correlations are observed among some parameters, owing to the misalignment between the optical axis and the z axis. Indeed, we checked that correlations among single parameters are small if the fit is performed in a reference frame aligned with the optical axis and emerge when the parameters are combined to get the position in the MEG II reference frame. These effects need to be taken into account when calculating the resolution for displacements along the normal direction to the target plane. An uncertainty propagation that includes the correlation between T_x and T_z gives, for instance, a resolution of 32 μm for displacements along the direction normal to the target plane, the most dangerous for the positron track angle measurements. The calculation of the eigenvalues and eigenvectors of the covariance matrix does not give indications of directions in

TABLE I. Example of the correlation matrix for a displacement of the target of 55 μm along the X axis with respect to the reference position. Translations are described by the three vector components of **T**. Rotations are described by three Euler angles according to the conventions used in the MEG II software.

	T_x	T_y	T_z	θ_1	θ_2	θ_3
T_x	1.000	−0.022	0.983	0.012	0.787	−0.006
T_y	−0.022	1.000	−0.022	0.005	−0.015	−0.010
T_z	0.983	−0.022	1.000	0.015	0.799	−0.011
θ_1	0.012	0.005	0.015	1.000	−0.001	−0.778
θ_2	0.787	−0.015	0.799	−0.001	1.000	0.006
θ_3	−0.006	−0.010	−0.011	−0.778	0.006	1.000

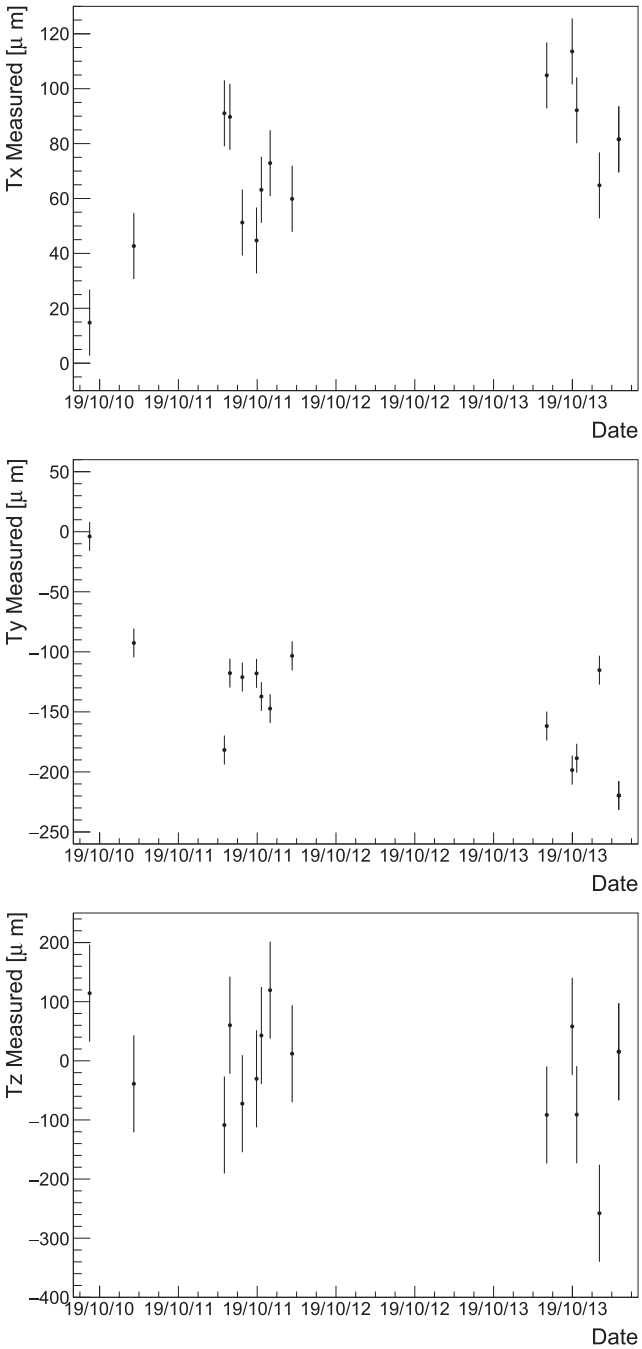

FIG. 14. Fitted T_x, T_y, and T_z for pictures taken during the 2019 MEG II engineering run.

the parameter space along which there is very poor resolution (*weak modes*).

V. MEASUREMENTS IN THE MEG II EXPERIMENT

We operated successfully the photo-camera during the MEG II 2018 and 2019 engineering runs. As an example, fit results for T_x, T_y, T_z, assuming the reference position as (0, 0, 0), are shown in Fig. 14 for a time interval of 1 day. The time interval with no measurement corresponds to cycles of extraction and insertion of the target.

VI. CONCLUSIONS

A photogrammetric method used for monitoring the target position during the MEG II data-taking run is presented. The method exploits imaging techniques to find displacements of patterns drawn on the target with respect to a reference picture taken at the beginning of a data-taking run. By combining this information with the results of an optical survey, it is possible to determine the position of the target during the run when the target is not accessible. The method described reaches the required resolution of less than 100 μm on the displacements along the axis normal to the target plane.

The photo-camera system has to be permanently installed inside the MEG II magnetic field volume and operated with the magnetic field on. Hence, it has been designed to avoid the presence of any ferromagnetic component. Moreover, a USB communication interface has been selected to avoid failure observed with an Ethernet interface during the first engineering data-taking run. Finally, the photo-camera will be placed at a sufficient distance from the beam axis in order to not interfere with the beam halo. All these features have been tested during the engineering MEG II runs in 2017–2019.

A bench-top test has been performed at INFN Roma with the same photo-camera of the final system in a geometrical arrangement that reproduces the setup inside the MEG II magnetic field. The accuracy of the measurement of the target displacement with respect to a reference picture has been measured to be $\sigma(\Delta x) = 12$ μm and $\sigma(\Delta z) = 82$ μm. Even in the worse situation of a large displacement of a few mm along the optical axis, the accuracy remains below the MEG II requirements. We also notice that the performances are significantly affected by the presence of large correlations between displacements along x and z. This could be significantly improved by combining the images of two photo-cameras looking at the target from two different points of view.

All these results make highly recommendable the installation of the system in the final setup of the MEG II experiment, with no evident interference with the rest of the apparatus. Eventually, a two-photo-camera analysis will be developed to improve the performances.

ACKNOWLEDGMENTS

We are grateful to our colleagues from the MEG II collaboration for their support in the development of this study.

DATA AVAILABILITY

The data that support the findings of this study are available from the corresponding author upon reasonable request.

REFERENCES

[1] M. Beker, G. Bobbink, B. Bouwens, N. Deelen, P. Duinker, J. van Eldik, N. de Gaay Fortman, R. van der Geer, H. van der Graaf, H. Groenstege *et al.*, "The Rasnik 3-point optical alignment system," J. Instrum. **14**, P08010 (2019).

[2] L. Ren, P. Shao, D. Zhao, Y. Zhou, Z. Cai, N. Hua, Z. Jiao, L. Xia, Z. Qiao, R. Wu *et al.*, "Target alignment in the Shen-Guang II Upgrade laser facility," High Power Laser Sci. Eng. **6**, e10 (2018).

[3] A. M. Baldini, E. Baracchini, C. Bemporad, F. Berg, M. Biasotti, G. Boca, P. W. Cattaneo, G. Cavoto, F. Cei, M. Chiappini *et al.*, "The design of the MEG II experiment," Eur. Phys. J. C **78**, 380 (2018).

[4] A. M. Baldini, Y. Bao, E. Baracchini, C. Bemporad, F. Berg, M. Biasotti, G. Boca, M. Cascella, P. W. Cattaneo, G. Cavoto *et al.*, "Search for the lepton flavour violating decay $\mu^+ \to e^+\gamma$ with the full dataset of the MEG experiment," Eur. Phys. J. C **76**, 434 (2016).

[5] G. Cavoto, A. Papa, F. Renga, E. Ripiccini, and C. Voena, "The quest for $\mu \to e\gamma$ and its experimental limiting factors at future high intensity muon beams," Eur. Phys. J. C **78**, 37 (2018).

[6] G. Chiarello, A. M. Baldini, G. Cavoto, F. Cei, M. Chiappini, A. Corvaglia, M. Francesconi, L. Galli, F. Grancagnolo, M. Grassi *et al.*, "The construction technique of the new MEG II tracker," Nucl. Instrum. Methods Phys. Res., Sect. A **936**, 495–496 (2019).

[7] A. M. Baldini, G. Cavoto, F. Cei, M. Chiappini, G. Chiarello, A. Corvaglia, M. Francesconi, L. Galli, F. Grancagnolo, M. Grassi *et al.*, "The ultra light drift chamber of the MEG II experiment," Nucl. Instrum. Methods Phys. Res., Sect. A **958**, 162152 (2020).

[8] D. Palo, M. Hildebrandt, A. Hofer, W. Kyle, D. Lad, T. Libeiro, and W. Molzon, "Precise photographic monitoring of MEG II thin-film muon stopping target position and shape," Nucl. Instrum. Methods Phys. Res., Sect. A **944**, 162511 (2019).

[9] J. Canny, "A computational approach to edge detection," IEEE Trans. Pattern Anal. Mach. Intell. **PAMI-8**, 679–698 (1986).

[10] P. V. C. Hough, "Machine analysis of bubble chamber pictures," Conf. Proc. C **590914**, 554–558 (1959).

[11] F. Zernike and F. J. M. Stratton, "Diffraction theory of the knife-edge test and its improved form, the phase-contrast method," Mon. Not. R. Astron. Soc. **94**, 377–384 (1934).